International Journal of Modern Manufacturing Technologies
ISSN 2067–3604, Vol. XIII, No. 1 / 2021

ANALYTICAL AND FEM SIMULATION STUDIES ON FRICTION RESISTANCES IN ANGULAR BALL BEARING

Jan Kosmol

Silesian University of Technology, Faculty of Mechanical Engineering, Department of Machine Technology
Konarskiego 18A, 44-100 Gliwice, Poland

Corresponding author: Jan Kosmol, jkosmol@polsl.pl

Abstract: The paper presents analytical and FEM results of friction resistances in angular ball bearing. Theoretical considerations concerning the motion in angular-ball bearing were presented in the article. It has been hypothesized that since the phenomenon of the bearing ball spinning, sliding and rolling can be observed in the angular- ball bearing, the resulting motion resistance can significantly affect the overall motion resistance due to the friction between the balls and bearing raceways. A simple mathematical relationship has been developed for the calculation of motion resistance due to the spinning, sliding and rolling phenomenon. Experimental studies of motion resistance in the ball bearing were conducted in order to verify the analytical model and obtained results confirmed adequacy of the developed models.

Key words: spin, sliding, rolling, motion resistance

1. INTRODUCTION

The development of HSC (High-Speed Cutting) technology requires, among others, machine tools that provide much higher kinematic parameters.
A significant increase in rotational speed results in the necessity of structural changes in bearing units. Rotational speed has a significant effect on the amount of heat that is generated in the bearings. The bearing unit constructor should have the tools that allow estimating the amount of heat generated in the bearing based on the load and rotational speed.
A significant difficulty in estimating the amount of heat in the bearing is the lack of computational models, which also consider the phenomena not mentioned in the classical theory of rolling bearings. One of them is friction sliding and spin phenomenon that accompanies the ball rolling along the bearing ring raceways (Jones, 1959), (Houpert, 1999).
Therefore, the main purpose of the article is to develop computational models that will enable the estimation of the motion resistance resulting from the various physical phenomena that occur in the rolling bearing. Knowledge of motion resistance and rotational speed of the bearing allows the analytical calculation of power losses in the bearing and thus the amount of heat that will be generated in the bearing.

2. MODEL OF KINEMATIC MOTION IN A BALL BEARING

Figure 1 shows schematically the angular ball bearing with the most important movements of the balls and the inner ring and the angles. It is assumed that the drive comes from the inner ringside while the outer ring is immobilized.
The basic rotational motion of the bearing (inner ring) at a speed ω causes the orbital motion of all the balls rolling on the inner ring raceway at an angular velocity ω_m and the rotational motion of the balls around their own axis inclined to the axis of the bearing at an pitch angle β, at the angular velocity ω_B.
As a result of the varied linear velocities at the contact points, the ball rotates around the normal axis concerning the contact area at the spin angular velocity ω_s.
The tangential velocities of the outer ring raceway are V_{1o} and of the ball V_{2o} at the contact point of outer ring differs. Similarly situation we observe at the contact point of the inner ring. As a result of that a sliding phenomenon between outer and inner rings and balls sliding speeds $V_{(T)so}$ (Figure 1(b)) and $V_{(T)si}$ occurs respectively.
Angular velocities ω_m, ω_B, and ω_s are kinematically related (Harris and Kotzalas, 2007). This is illustrated in Figure 1(c), which shows a kinematic triangle formed by those three vectors.
Sliding velocities $V_{(T)so}$ and $V_{(T)si}$ and spin velocities V_{so} and V_{si} causes sliding friction.
Gyroscopic angular velocity ω_g causes sliding friction too, but in this paper, the phenomenon will be omitted because it occurs in very high speed only.
In the next chapters, the sliding, rolling and spin phenomenon will be explained in detail for the point of view of resistance motion of angular ball bearing.

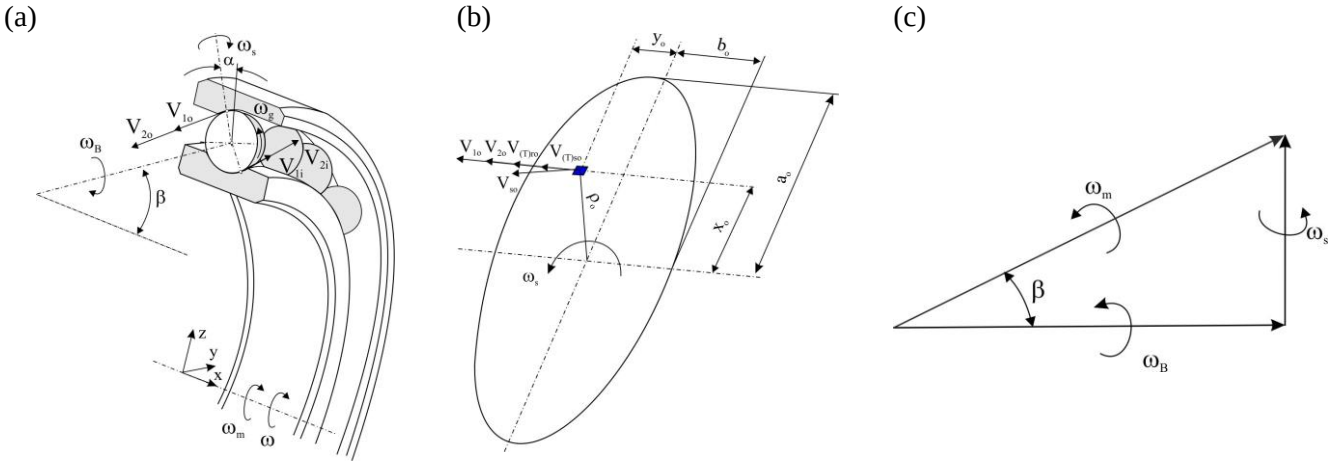

Fig. 1. View of the angular ball bearing with the indicated most important movements of the ball and the bearing ring (a), view of contact deformation between a ball and outer ring and velocity distribution (b), kinematic triangle of angular velocity (Harris and Kotzalas, 2007) (c): ω - angular velocity of the inner ring [s^{-1}], ω_m - angular velocity in the orbital motion of the balls [s^{-1}], ω_B – angular velocity of the balls rolling motion [s^{-1}], ω_s - angular velocity of the balls as a result of the spin phenomenon [s^{-1}], ω_g - angular velocity of the balls as a result of gyroscopic phenomenon [s^{-1}], α - contact angle [^{0}], β - ball pitch angle [^{0}], V_{1o}, V_{2o} – tangential velocity of the outer ring and ball [mm/s], $V_{(T)so}$, – tangential velocity due to sliding [mm\s], V_{so}, – tangential velocity due to spinning [mm/s], $V_{(T)ro}$, – tangential velocity due to rolling [mm/s], ρ_o – radius [mm], a_o, b_o – semi-major and semi-minor axis [mm]

3. THE SLIDING PHENOMENON IN AN ANGULAR BALL BEARING

This chapter will present models to calculate analytically the slip speed in the ball contact area with the outer raceway $V_{(T)so}$ and with an internal raceway $V_{(T)si}$. It is essential to know these speed to determine the resistance to motion caused by sliding friction in a rolling bearing. Basic formulas for calculating linear velocities V_{1o}, V_{1i}, V_{2o}, V_{2i} and slip velocities $V_{(T)so}$, $V_{(T)si}$ were presented by Jones (Jones, 1959). The author adopted them for his research.

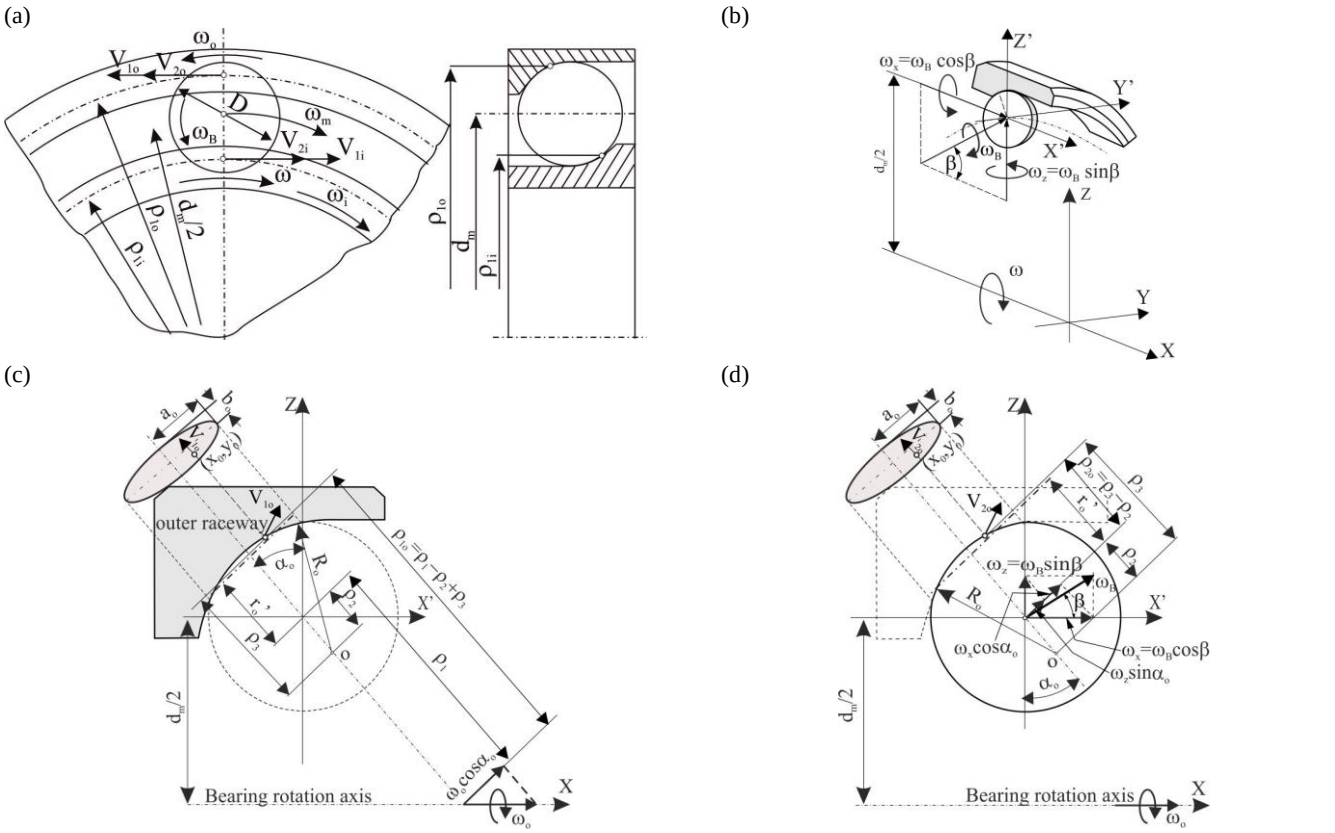

Fig. 2. Kinematic and geometric assumptions for determining the tangential velocity $V_{(T)so}$ at the contact site of the ball and outer raceway: ω_o, ω_i – angular velocity of the outer and inner ring [s^{-1}], α_o – outer contact angle, d_m - pitch diameter of the bearing [mm], r_o' – pure radius of ball rolling [mm], R_o – raceway curvate radius [mm]

We will use Figure 2(a), which shows the linear velocities V_{1o}, V_{1i}, V_{2o}, V_{2i}. Figure 2(b), Figure 2(c), Figure 2(d) (Jones, 1957) shows the speed vectors ω_o and ω_B and their components in the area of cooperation of the ball with the outer raceway.
The geometrical quantities are also presented, which allow calculating the peripheral velocities V_{1o} and V_{2o}. Figure 2(a) presents the method of determining the peripheral speed of the raceway V_{1o} at any point on the contact ellipse (x_0, y_0) as a result of the rotation of the outer ring at angular velocity $\omega_o \cos\alpha_o$ within ρ_{1o}. Figure 2(b) and Figure 2(c) show how to determine the circumferential velocity of the V_{2o} ball at any point on the contact ellipse (x_0, y_0) as a result of the rotating motion of the ball at angular velocity ω_B within ρ_{2o} (Harris and Kotzalas, 2007).

$$V_{1o} = -\omega_o \rho_{1o} \cos\alpha_o = -\frac{d_m}{2}\omega_o - \left(\sqrt{R_o^2 - x_0^2} - \sqrt{R_o^2 - a_o^2} + \sqrt{\left(\frac{D}{2}\right)^2 - a_o^2}\right)\omega_o \cos\alpha_o \quad [\frac{mm}{s}] \quad \text{(Jones,1959)}$$

$$V_{2o} = -\omega_B \rho_{2o} \cos(\alpha_o - \beta) = -\omega_B \left(\sqrt{R_o^2 - x_0^2} - \sqrt{R_o^2 - a_o^2} + \sqrt{\left(\frac{D}{2}\right)^2 - a_o^2}\right)\cos(\alpha_o - \beta) \quad [\frac{mm}{s}] \quad \text{(Jones,1959} \tag{1}$$

The slip speed $V_{(T)so}$ in the contact area of the ball with the outer raceway is defined as (Jones, 1959).

$$V_{(T)so} = V_{1o} - V_{2o} = -\frac{d_m}{2}\omega_o - (\omega_o \cos\alpha_o - \omega_B \cos(\alpha_o - \beta))\left(\sqrt{R_o^2 - x_0^2} - \sqrt{R_o^2 - a_o^2} + \sqrt{\left(\frac{D}{2}\right)^2 - a_o^2}\right) \quad [\frac{mm}{s}] \tag{2}$$

where: ω_o - angular relative velocity of the ball and outer ring.

Similar reasoning may be used to determine the slip speed $V_{(T)si}$ in the contact area of the ball with the inner raceway.
The considerations presented so far show that the phenomenon of balls rolling on raceways is accompanied by the phenomenon of their slippage. Therefore, for a complete picture of these phenomena, it is advisable to determine also the peripheral velocity in the pure rolling of balls. It is assumed that this rolling takes place on the radius marked in Figure 2 as r_o' (for the inner ring it will be r_i'). The peripheral speed of pure rolling measured on the outer ring $V_{(T)ro}$ will be (Jones, 1959)

$$V_{(T)ro} = -\omega_o(0.5d_m + r_o' \cos\alpha_o) \quad [\frac{mm}{s}] \tag{3}$$

For the inner race $V_{(T)ri}$ looks similary.
The pure rolling radii of r_o' , r_i' can be determined from the condition $V_{(T)si} = 0$ or $V_{(T)so} = 0$. Then, for $x_o = a_{o1}$ (Figure 3(a)) for the outer ring the geometrical conditions (Figure 2(c)) occur:

$$r_o' = \sqrt{R_o^2 - a_{o1}^2} - \sqrt{R_o^2 - a_o^2} + \sqrt{\left(\frac{D}{2}\right)^2 - a_o^2} \quad [mm] \tag{4}$$

where: a_{o1} - coordinates in axis x for one of the pure rolling points, for the outer ring (Figure 3(a))

a) b)

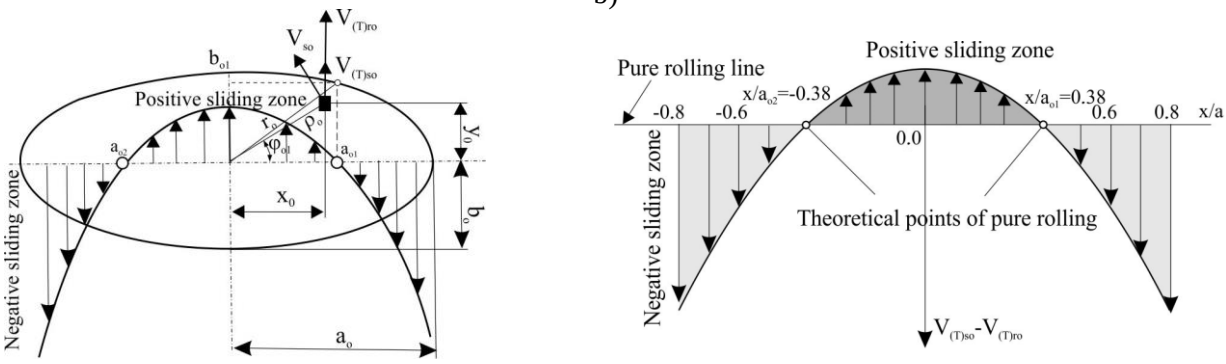

Fig. 3. Example of the distribution of the difference in sliding speed $V_{(T)so}$ and rolling speed $V_{(T)ro}$ for the test bearing FAG B7013-E (bearing speed n=12.000 rpm) in the contact area of the outer raceway with the ball

Coordinates a_1 and a_2 (the coordinate of a possible second point of pure rolling) can be estimated based on Houpert's theory (Houpert, 1999). According to this theory, points a_1/a and a_2/a describe the place of occurrence of pure rolling (Figure 3(a)). For the ORC (Outer Race Control) hypothesis (Jones, 1959), Houpert has shown that there is an identity

$$\frac{a_1}{a} = -\left(\frac{a_2}{a} + \frac{2R_a}{a} \frac{D\sin\alpha}{d_m} \right) \tag{5}$$

where: R_a -. equivalent radius of curvature ($R_a \approx D/2$). For a symmetrical system a_2 = abs(a_1), which occurs when we ignore the influence of gyroscopic phenomena, we obtain:

$$\left|\frac{a_1}{a}\right| + \frac{a_2}{a} = 2\left|\frac{a_1}{a}\right| = \frac{2R_a}{a} \frac{D\sin\alpha}{d_m} \tag{6}$$

The Figure 3(b) shows coordinates a_{o1} and a_{o2} for a test bearing FAG B7013-E, for rotational speed 12.000 rpm (Kosmol, 2016). In the zone of the contact ellipse x/a<-0.38 and x/a>0.38 there is a classic slip, called a negative slip, which is a source of sliding friction resistance during ball rolling. And in the zone -0.38<x/a<0.38 there is a so-called positive slip, which does not cause any resistance in movement.

Determining sliding velocities $V_{(T)si}$ and $V_{(T)so}$ requires knowledge of the geometrical dimensions of the bearing such as d_m, D, R_i, R_o, half-axis a_i and a_o of the contact ellipses, contact angles α_i and α_o and above all, angular velocities ω_i, ω_o,ω_m, ω_B. Analytical models for calculating velocities ω_i, ω_o, ω_m, ω_B will be presented further based on angular velocity ω.

Angular velocity ω_B is one of the most important information. It may be computed assuming that tangential velocities $V_{(T)ro}$ for pure rolling in the contact zone are equal, and for the outer ring (Jones, 1959).

$$\frac{\omega_B}{\omega_o} = \frac{\rho_1 + r_o'}{r_o'} \frac{\cos\alpha_o}{\cos(\alpha_o - \beta)} \tag{7}$$

or for the inner ring

$$\frac{\omega_B}{\omega_m} = -\frac{\rho_1 - r_i'}{r_i'} \frac{\cos\alpha_i}{\cos(\alpha_i - \beta)} \tag{8}$$

Assuming, that outer ring is immobile angular velocities of the inner and outer ring relative to the orbital motion of the balls ω_i, ω_o may be computed as follow:

$$\begin{aligned} \omega_o &= -\ \omega_m \quad [s^{-1}] \\ \omega_i &= \omega - \omega_m \quad [s^{-1}] \end{aligned} \tag{9}$$

Finally

$$\begin{aligned} \frac{\omega_B}{\omega} &= -\frac{1}{\frac{r_o'}{\rho_1 + r_o'} \frac{\cos(\alpha_o - \beta)}{\cos\alpha_o} + \frac{r_1'}{\rho_1 - r_1'} \frac{\cos(\alpha_i - \beta)}{\cos\alpha_i}} \\ \frac{\omega_m}{\omega} &= \frac{1}{1 + \left(\frac{\rho_1 + r_o'}{\rho_1 - r_i'} \right) \frac{r_i'}{r_o'} \frac{\cos\alpha_o}{\cos\alpha_i} \frac{\cos(\alpha_i - \beta)}{\cos(\alpha_o - \beta)}} \end{aligned} \tag{10}$$

Knowledge of speeds ω_B and ω_m allows you to calculate slip and rolling speeds $V_{(T)so}$, $V_{(T)si}$ $V_{(T)ro}$, $V_{(T)ri}$. Very similar models of ω_B and ω_m are met in literature, for example (Jones, 1959),(Harris and Kotzalas, 2007), (Noel at all, 2013).

Author proposed to introduce markings:

$$\begin{aligned} L_o &= \frac{d_m}{2} + \frac{d_m}{2r_o'} \cos\alpha_o \left(\sqrt{R_o^2 - a_o^2} - \sqrt{\left(\frac{D}{2}\right)^2 - a_o^2} \right) \quad [mm] \\ M_o &= 1 + \left(\frac{\frac{0.5d_m}{\cos\alpha_o} + r_o'}{\frac{0.5d_m}{\cos\alpha_i} - r_i'} \right) \frac{r_i'}{r_o'} \frac{\cos\alpha_o}{\cos\alpha_i} \frac{\cos(\alpha_i - \beta)}{\cos(\alpha_o - \beta)} \\ L_i &= \frac{d_m}{2} - \frac{d_m}{2r_i'} \cos\alpha_i \left(\sqrt{R_i^2 - a_i^2} - \sqrt{\left(\frac{D}{2}\right)^2 - a_i^2} \right) \quad [mm] \\ M_i &= \frac{M_o}{M_o - 1} \\ M_B &= \frac{r_o'}{\rho_1 + r_o'} \frac{\cos(\alpha_o - \beta)}{\cos\alpha_o} + \frac{r_1'}{\rho_1 - r_1'} \frac{\cos(\alpha_i - \beta)}{\cos\alpha_i} \end{aligned} \tag{11}$$

the tangential velocities $V_{(T)so}$, $V_{(T)si}$ looks like follow:

$$\begin{aligned} V_{(T)so} &= \left(\frac{L_o}{M_o} - \frac{\frac{d_m}{2r_o'} \cos\alpha_o \sqrt{R_o^2 - x_{0_o}^2}}{M_o} \right) \omega \quad [\frac{mm}{s}] \\ V_{(T)si} &= \left(\frac{L_i}{M_i} - \frac{\frac{d_m}{2r_i'} \cos\alpha_i \sqrt{R_i^2 - x_{0_i}^2}}{M_i} \right) \omega \quad [\frac{mm}{s}] \end{aligned} \tag{12}$$

and depend on the x_0 (x_{0o} for outer and x_{0i} for the inner race) co-ordinates only.

Figure 4(a) shows examples of tangential velocities $V_{(T)so}$, $V_{(T)si}$ as a function of the rotational speed of the bearing for the preload 1000N and co-ordinate x_0 equal 0.0 mm, 1.0 mm and 1.4 mm and Figure 4(b), as a function of x_0 co-ordinate.

The sliding velocities increase as you move away from the center of the contact ellipse x_0=0 (Figure 4(b)), reaching its highest values on the edges of the contact ellipse (x_0=a_o and a_i).

It should be noted that the sliding velocities change the sign (direction) of the ball sliding on the inner and outer raceways for x_0<=0.4 mm. For x_0=0.4 mm we can say about pure rolling of the ball (Figure 3).

If the sign of the slip changes, it means that we are in the zone of the so-called positive slip (Figure 3) in which there is no frictional resistance. Therefore, when calculating the motion resistance due to slip friction only those areas of the contact ellipse where negative slip occurs should be taken into account.

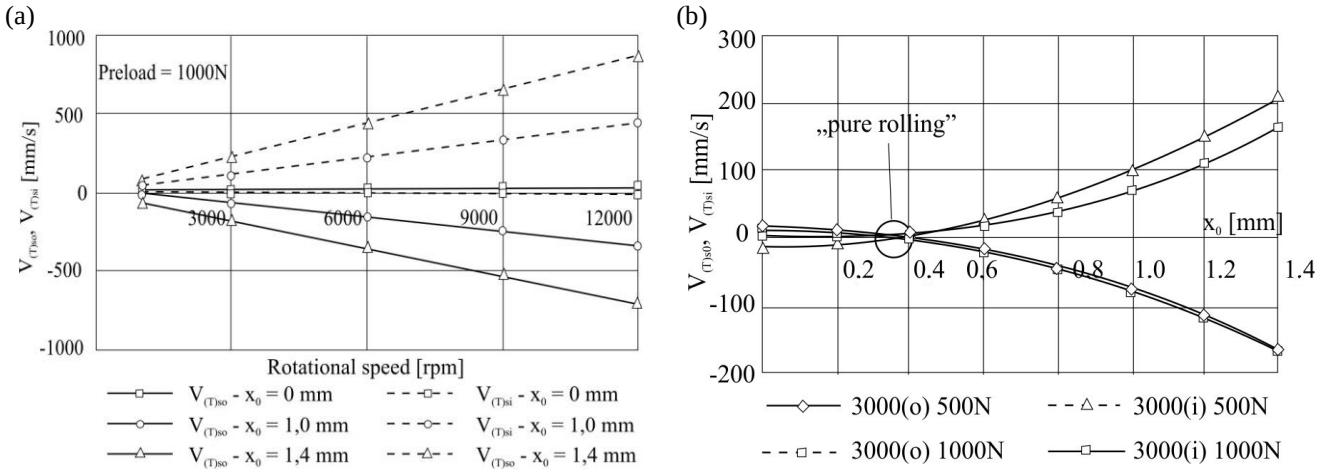

Fig. 4. Examples of tangential velocities $V_{(T)so}$, $V_{(T)si}$ as a function of a) rotational speed b) x_0 co-ordinate: (o) - for the outer ring, (i) – for the inner ring

4. SPINNING PHENOMENON IN AN ANGULAR BALL BEARING

As already shown in Figure 1 in an angular ball bearing occurs Spin phenomenon due to spin velocity ω_s. Determining spin speed ω_s is difficult. Figure 5(a) shows the kinematic assumptions that allow determining the angular velocity of the spin ω_{so} at the contact site of the ball and outer raceway (Jones, 1957). It was assumed that the relative velocity of the outer ring relative to the balls orbital motion at the velocity ω_m is ω_o (ω_o = - ω_m for immobile outer ring).

The ball orbital motion at the velocity ω_m rolls on the raceways at the velocity ω_B (Figure 2(a) and Figure 2(b)).

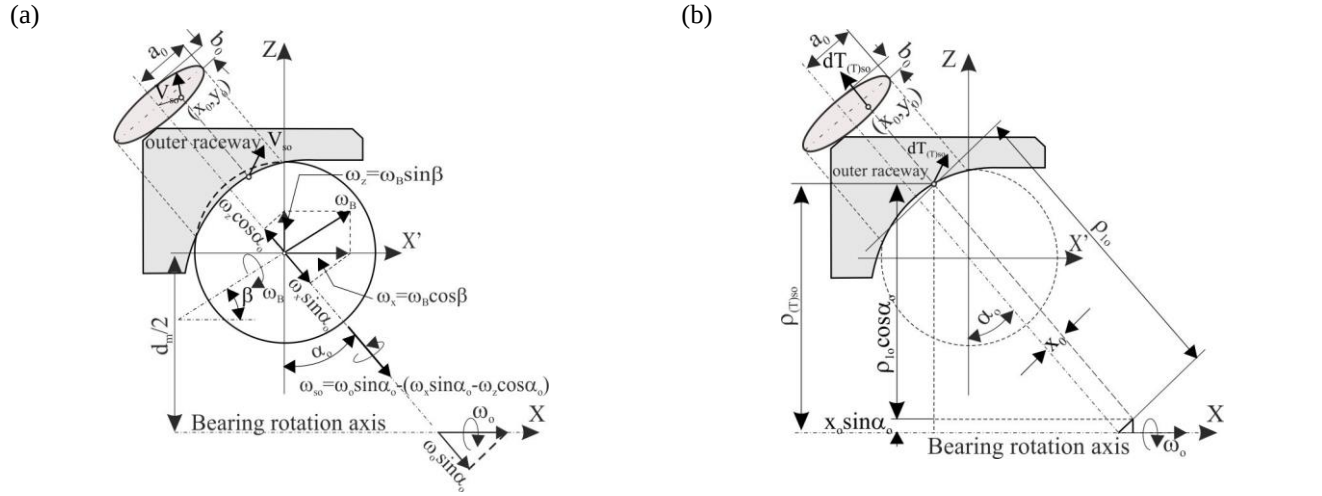

Fig. 5. Kinematic and geometric assumptions for determining the spinning velocity V_{so} at the contact site of the ball and outer raceway (a) and the definition of radius $\rho_{(T)so}$ of the ball sliding along the outer raceway (b)

Jones (Jones 1957) proposed to divide the rolling speed of ball ω_B into two components: ω_x and ω_z, consistent with the direction of the coordinate system. Both of those components are decomposed into components corresponding to the spin axis (Figure 5(a)) ($\omega_x \sin\alpha_o$ and $\omega_z \cos\alpha_o$).

The relative angular velocity of the outer ring ω_o also includes a component that affects the speed of the spin ($\omega_o \sin\alpha_o$, Figure 5(a)). As a result, the speed of spin at the contact point of the ball with the outer raceway ω_{so} is the sum of the three listed components. Similar reasoning can be made for an inner ring that rotates at a relative velocity ω_i.

Considering the determinations in Figure 5(a), the spin speeds ω_{si} and ω_{so} can be expressed as follows (Harris and Kotzalas, 2007):

$$\begin{aligned} \omega_{so} &= \omega_B \sin(\alpha_o - \beta) - \omega_o \sin\alpha_o \quad [s^{-1}] \\ \omega_{si} &= -\omega_B \sin(\alpha_i - \beta) + \omega_i \sin\alpha_i \quad [s^{-1}] \end{aligned} \tag{13}$$

where: ω_{si}, ω_{so} - relative spin velocities of in the area of contact with the inner and outer ring.

Inserting (10) and (11) to (9) we obtain:

$$\omega_i = \frac{\omega}{M_i} \quad [s^{-1}]; \qquad \omega_o = -\frac{\omega}{M_o} \quad [s^{-1}] \tag{14}$$

Calculating the velocity ω_B also requires knowing the bearing angles α_i and α_o. Because it is necessary to know the velocity ω_B to determine the angles α_i, α_o of bearing operation, and to determine this velocity it is necessary to know the angle β, the solution of the spin issue requires iterative methods.

The spin phenomenon, is not fully investigated. Therefore, in the literature, several hypotheses simplify the designation of, among others, the angle β and the spin speed ω_s. The view of the relationships of this velocity with the angle β is presented in (Noel at all, 2013).

One of most popular is the Outer raceway control (OCR) hyphotese. Depending on the assumed hypothesis, we obtain different values of the angle β and thus the spin speed ω_s. We will continue to use the one of most popular hyphotese the Outer raceway control (OCR). For such a hypothesis, assuming $\omega_{so}=0$, we can compute the angle β as follow:

$$tg\beta \approx \frac{\sin\alpha_o}{\cos\alpha_o + \frac{D}{d_m}} \tag{15}$$

(Houpert, 1999) as opposed to numerical simulation has developed an analytical model that should allow the reader to better predict the bearing kinematics. Most important is the calculation of the location of the pure rolling line on the contact ellipse, because they make possible to calculate the velocity ω_B more precisely.

The author carried out experimental verification tests for the type FAG7OB13-E bearing. For such a bearing he determined the relative speed of ω_{si} according to relationship (13). Input data for the analysis was taken from (Kosmol, 2016). Figure 6 presents the results for two values of preload, which is no less important thant speed (Zama at all, 2019).

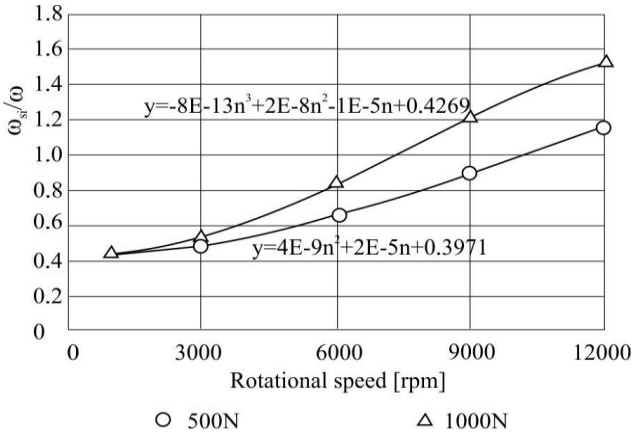

Fig. 6. Influence of rotational speed of the bearing on spin speed ω_{si}/ω for two preloads: 500N and 1000N; n – rotational speed [rpm]

Regression models presented in Figures 6 will be used to calculate the resistance due to the spin phenomenon.

5. CALCULATION MODELS OF MOTION RESISTANCES IN A ROLLING BEARING

The main objective of the present study is to demonstrate the validity of the thesis that the components resulting from the spin phenomenon, sliding and rolling of balls significantly contributes to the motion resistance of the rolling bearing and to develop analytical calculation models that would allow to estimate those resistances based on the knowledge of the rotational speed of the bearing, its preload and external load.

The motion resistance in the rolling bearing in the most general case results from:

$$M_T = \left(M_{T(r)} + M_{T(s)} + M_s^* + M_{ext}\right) + M_v \quad [Nmm] \tag{16}$$

where: M_T - friction torque on the drive shaft,
$M_{T(r)}$ – friction torque due to rolling movement,
$M_{T(s)}$ - friction torque due to sliding movement,
M^*_s – friction torque due to spinning effect, reduced onto the drive shaft,
M_{ext} –friction torque due to external loads,
M_v – friction torque due to lubrication.

The motion resistance resulting from the external load $M_{ext,}$ and lubricatio M_v can be estimated based on models available in the literature (Palmgren, 1951),(Harris and Kotzalas, 2007), (Kosmol, 2016).

A procedure will be introduced to obtain mathematical formulas that would calculate the motion resistance due to the spin phenomenon, rolling and sliding as a function of the rotational speed and preload.

5.1 The motion resistance due to the spinning effect

Figures 7(a) shows the hypothetical distribution of normal stresses (pressures) in the area of contact between the two surfaces that will occur at the contact site of the ball and the raceway of the bearing. This is a characteristic distribution for the Hertz theory, where the area of contact deformation takes the form of an ellipse with the semi-axes a and b, and the maximum stress occurs in the centre of the ellipse.

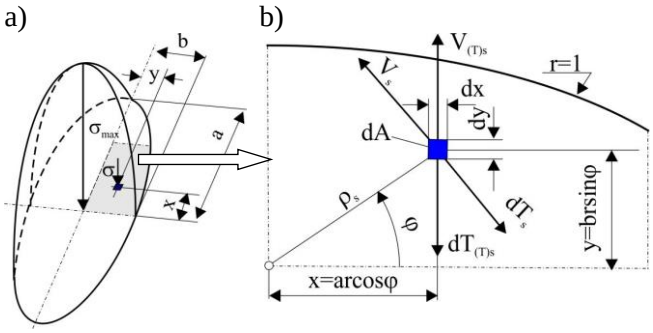

Fig. 7. Normal stress distribution in the contact area (a), spinning V_s, sliding $V_{(T)s}$ velocities and elementary friction load dT (dT_s, $dT_{(T)s}$) (b), r, φ - elliptic coordinates

Such a distribution of normal stresses is described by the Hertz model:

$$\sigma(x,y)=\frac{1.5Q}{\pi ab}\sqrt{\left(1-\left(\frac{x}{a}\right)^2-\left(\frac{y}{b}\right)^2\right)} \tag{17}$$

Normal stress σ is the source of the elemental spinning and sliding friction load dT (dT_s, $dT_{(T)s}$) at the point (x,y), according to the Columbus model:

$$dT=\mu\sigma(x,y)dA=\mu\sigma(x,y)dxdy \tag{18}$$

Friction load T across the entire contact area of the two surfaces is the surface integral, namely:

$$T=\mu\iint_A\sigma(x,y)dA=\mu\iint_A\sigma(x,y)dxdy \tag{19}$$

It is more convenient to solve the elliptic integral (19) by entering elliptic coordinates $x=ar\cos\varphi$, $y=br\sin\varphi$ (Figure 7(b)).

Considering in (19) the dependencies (17) and (18), the friction load T takes the following form:

$$T=\frac{1.5Q\mu}{\pi}\int_0^1\int_0^{2\pi}\sqrt{1-r^2}\,rdrd\varphi=3Q\mu\int_0^1 r\sqrt{1-r^2}dr=$$
$$T=Q\mu\ \ [N] \tag{20}$$

The elemental friction load dT_s on the arm ρ_s (Figure 7(b)) generates an elementary friction moment dM_s,

$$dM_s=\rho_s dT_s=\mu\rho_s\sigma(x,y)dA$$
$$\rho_s=\sqrt{x^2+y^2}=r\sqrt{a^2\cos^2\phi+b^2\sin^2\phi}\quad [mm] \tag{21}$$

Friction torque M_s due to spinning effect is an elliptic integral on the contact surface,

$$M_s=\frac{1.5Q\mu}{\pi ab}\int_0^1\int_0^{2\pi}\rho_s\sqrt{1-r^2}\,abrdrd\varphi=\frac{1.5Qa\mu}{\pi}\int_0^1\int_0^{2\pi}r^2\sqrt{1-r^2}\sqrt{\cos^2\varphi+\left(\frac{b}{a}\right)^2\sin^2\varphi}d\varphi dr\quad [Nmm] \tag{22}$$

Since the integral $\int_0^1 r^2\sqrt{1-r^2}dr=\frac{\pi}{16}$ and the integral $\int_0^{\pi/2}\sqrt{\cos^2\varphi+\left(\frac{b}{a}\right)^2\sin^2\varphi}\approx\frac{\pi}{3}$ (Author solved the integral numerically for b/a=0.02-0.1 because he proved that b/a <<1 (Kosmol, 2016)) hence the friction torque due to spinning effect M_s is:

$$M_s\approx\frac{\pi Qa\mu}{8}\quad [Nmm] \tag{23}$$

The friction torque due to the spinning effect as one of the components of motion resistance in the rolling bearing (16) appears on the drive shaft in the form of the M^*_s torque, i.e. the torque reduced onto the drive shaft. The reductions of the friction torque can be based on the principle of conservation of energy or the principle of the equivalence of the energy supplied and the work done, in this case - the friction work. Hence the equivalence:

$$M^*_s\omega=M_s\omega_s \tag{24}$$

The methodology of determining spin speed ω_{si} is described in Chapter 3 (dependence (13) or regression models shown in Figure 6).

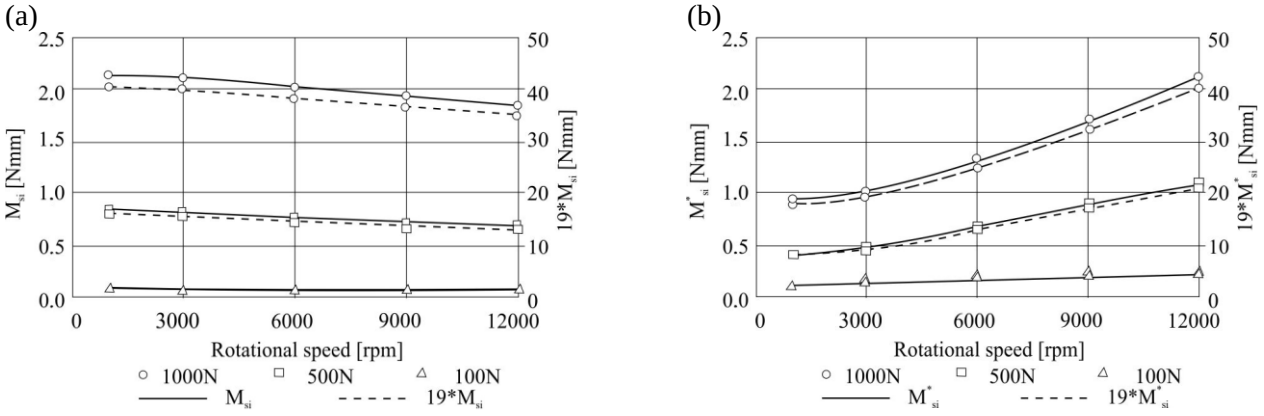

Fig. 8. Effect of rotational speed on the friction torque due to the spinning effect on inner ring M_{si} (a), after reduction to the drive shaft M^*_{si} (b); 19 – number of balls

Within the speed range of 1000 - 12000 rpm and the preload 100N-1000N, the friction torques due to spinning effect M_{si} and M^*_{si} for the bearing type FAG 7OB13-E are shown at Figure 8. Figure 8 does't show any resistance due to the spin phenomenon on the outer raceway because the ORC hypothesis was adopted.

5.2 The motion resistance due to the sliding effect

To calculate the motion resistance due to the sliding effect the contact area should be divided into the sliding and rolling part (Figure 9).The elemental friction load $dT=dT_{(T)so}=dT_{(T)s}$ (Figure 5(b), Figure 9) due to sliding speed $V_{(T)s}$ (Figure 7(b)) of the balls generates a torque $dM_{(T)s}$ too, because of the arm $\rho_{(T)s}$ ($\rho_{(T)so}$ at Figure 5(b)):

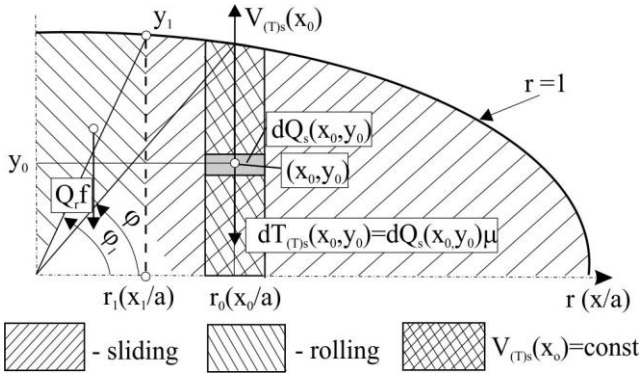

Fig. 9. Definition of elementary sliding $dT_{(T)s}(x_o,)$, rolling $Q_r f$ friction load, elementary contact force $dQ_s(x_0)$ and sliding velocity $V_{(T)s}(x_0)$ at point (x_o,y_o); r, φ - elliptic coordinates, f – coefficient of friction

$$dM_{(T)s} = \rho_{(T)s} dT = \mu \rho_{(T)s} \sigma(x,y)\, dA \qquad (25)$$

The calculation of the elementary moment $dM_{(T)s}$ is easier using the equation of the elementary friction power of a ball with a raceway and the corresponding elementary power on the drive shaft, namely:

$$V_{(T)s}\, dT = \omega\, dM_{(T)s} \qquad (26)$$

Inserting dependences $V_{(T)so}$ (2), $\sigma(x,y)$ (17) and $dT_{(T)so}$ (18) to (26) we obtain an elementary moment $dM_{(T)so}$ for the outer raceway.

The same can be done for the inner raceway, and calculate the elementary moment dM(T)si.

The total torque M(T)s is an integral part of the contact ellipse surface.

Integrating the relations (27) must be carried out over the area of the contact ellipse where negative slip occurs (Figure 4(b), Figure 9) within the boundaries only for one (first) quarter:

$$dM_{(T)so} = \frac{1.5 Q_o \mu}{\pi a_o b_o} \sqrt{1-\left(\frac{x_o}{a_o}\right)^2 - \left(\frac{y_o}{b_o}\right)^2} \left(\frac{L_o}{M_o} + \frac{\frac{d_m}{2r_o'} \cos\alpha_o \sqrt{R_o^2 - x_o^2}}{M_0} \right) dxdy \qquad (27)$$

$$x \in (x_1, a); y \in (0,\ y_1);\ r \in (r_1, 1);\ \varphi \in (\varphi_1, \pi/2); \qquad (28)$$

Then the total moment $M_{(T)so}$ is as follows:

where the r and φ_1 is explained in Figure 9.

$$M_{(T)so} = 4 \frac{1.5 Q_o \mu}{\pi a_o b_o} \int_{x_{1o}}^{a_o} \int_{0}^{y_{1o}} \sqrt{1-\left(\frac{x_o}{a_o}\right)^2 - \left(\frac{y_o}{b_o}\right)^2} \left(\frac{L_o}{M_o} + \frac{\frac{d_m}{2r_o'} \cos\alpha_o \sqrt{R_o^2 - x_o^2}}{M_0} \right) dxdy \quad [Nmm] \qquad (29)$$

and after introducing elliptic coordinates

$$M_{(T)so} = \frac{6 Q_o \mu}{\pi a_o b_o} \int_{r_{1o}}^{1} \int_{0}^{\varphi_1} a_o b_o r \sqrt{1-r^2} \left(\frac{L_o}{M_o} - \frac{\frac{d_m}{2r_o'} \cos\alpha_o \sqrt{R_o^2 - (ar)^2 \cos^2\varphi}}{M_o} \right) dr d\varphi \quad [Nmm] \qquad (30)$$

To explain how to integrate the dependence (30) we will use Figure 9. In the analysis carried out in chapter 3 covering the slip speed on $V_{(T)s}$, it is assumed that it is only a function of a coordinate x_0. This means that the slip speed do not change along the axis y. However, the assumed distribution of normal pressures (Hertz model (17)) shows that they will change with the coordinates x as well as y. Therefore, to determine the elementary contact force $dQ_s(x_0,y_0)$ and then the elementary frictional force $dT_{(T)s}(x_0,y_0)$ in point (x_0,y_0) there is a need carry out the integration of pressures within the range of $y=0$ to $y=y_1$ and using the elliptical coordinates within $r=r_1$ to 1.

It should be done for outer and inner rings.

It can be demonstrated that the integration results will be expressions:

$$M_{(T)so}=\frac{2Q_o\mu\varphi_1\left(\sqrt{1-r_{1o}^2}\right)^3}{\pi}\left(\frac{L_o}{M_o}-\frac{6\frac{d_m}{2r_o}\cos\alpha_o}{M_o}\right)\approx\frac{2Q_o\mu\varphi_1\left(\sqrt{1-r_{1o}^2}\right)^3}{\pi}\left(\frac{L_o}{M_o}-\frac{6\frac{d_m}{D}\cos\alpha_o}{M_o}\right)\quad[Nmm]$$
$$M_{(T)si}=\frac{2Q_i\mu\varphi_1\left(\sqrt{1-r_{1i}^2}\right)^3}{\pi}\left(\frac{L_i}{M_i}-\frac{6\frac{d_m}{2r_i}\cos\alpha_i}{M_i}\right)\approx\frac{2Q_i\mu\varphi_1\left(\sqrt{1-r_{1i}^2}\right)^3}{\pi}\left(\frac{L_i}{M_i}-\frac{6\frac{d_m}{D}\cos\alpha_i}{M_i}\right)\quad[Nmm]\tag{31}$$

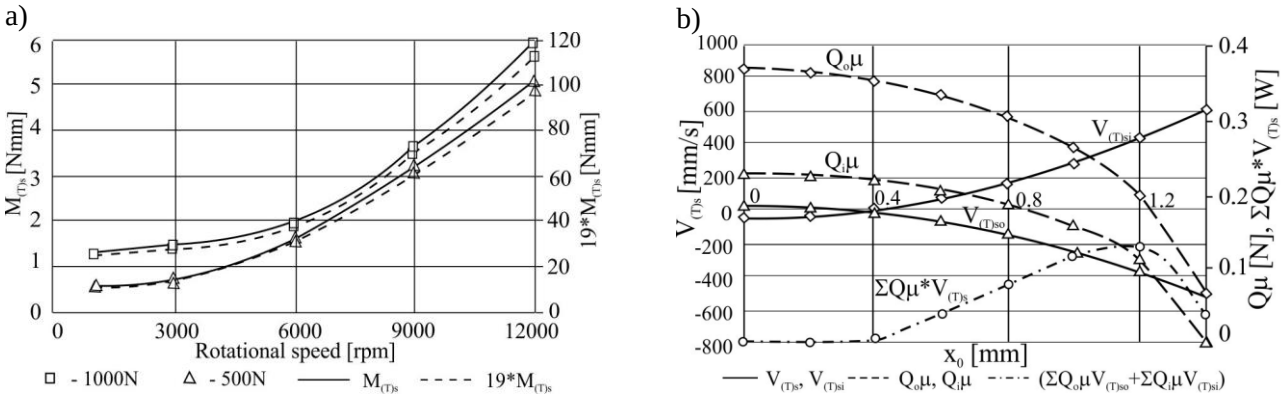

Fig. 10. Effect of the rotational speed on the sum of friction torques on inner and outer races $M_{T(s)}$ (a) and effect of x_0 co-ordinate on the sliding speed $V_{(T)so}$, $V_{(Tsi)}$, friction load $Q_o\mu$, $Q_i\mu$ and power of friction $\Sigma Q\mu*V_{(T)s}=\Sigma Q_o\mu*V_{(T)so}+\Sigma Q_i\mu*V_{(T)si}$ for 9.000 rpm (b): 19 – number of balls in the bearing

Figure 10(a) presents some exemplary results of analyses in the form of the relation of the sum of the moments of resistance $M_{T(s)}=M_{(T)so}+M_{(T)si}$ in the function of rotational speed and preload of bearings. Calculations were carried out for the extended angular bearing model (Kosmol, 2019). Figure 10 allows the following statements to be made:

- Increased rotational speed and increased bearing preload increase the torque resistance.
- In the courses of the power of friction $\Sigma Q\mu*V_{(T)s}$, there is a maximum, around the co-ordinates x_0=1,2.
- The sliding speed $V_{(T)so}$, $V_{(T)si}$, friction load $Q_o\mu$, $Q_i\mu$ and power of friction $\Sigma Q\mu*V_{(T)s}$ depends on the position of the contact ellipse (x_0 co-ordinate). Minimum value of $V_{(T)so}$, $V_{(T)si}$ occurs near the centre but maximum value at the border of the ellipse.
- Maximum value of friction loads $Q_o\mu$, $Q_i\mu$ occurs near the centre and close to zero at the border.
-The power loss of friction $\Sigma Q\mu*V_{(T)s}=\Sigma Q_o\mu*V_{(T)so}+\Sigma Q_i\mu*V_{(T)si}$ changes nonmono-tonically, respectively to the changes of the co-ordinate x_0.

5.3 The motion resistance due to the rolling effect

The problem with estimating rolling friction resistance in rolling bearings results from the fact that apart from them there are also sliding friction resistances, and since friction resistances are generally proportional to normal pressures occurring between the ball and raceways, it is not known which part of these pressures contributes to rolling friction and which to sliding friction.

In chapter 3, after Houpert (Houpert, 1999), a theory was quoted, according to which in the area of contact between a ball and treadmills there are rolling circles, followed by pure rolling. Theoretically, this means that the contact of the ball with the raceways is an area of very little space. In this case, the rolling friction resistance is close to zero, as almost all surface pressure will occur in the sliding area of the balls on the raceways.

The author proposes the calculation of rolling friction resistance in the area where, according to Houpert (Houpert, 1999), positive slip occurs, i.e. one that does not introduce sliding friction resistance. Such an area has a certain contact area and it is possible to estimate the surface pressure, and thus the contact load, which, together with the coefficient of rolling friction, will make it possible to estimate the rolling friction resistance. Figure 9 shows areas of such assuming.

Motion resistance $M_{T(r)}$ due to the ball rolling on raceways must be determined according to a different rule than for ball slippage. This is due to the definition of the coefficient of rolling friction f which has a dimension of length. Author (Kosmol, 2018) presented a proposal for the analytical determination of the coefficient of rolling friction f as a function of contact load Q.

The frictional resistance due to rolling is as follow:

$$M_{(T)r} = Q_r f \quad [Nmm] \tag{32}$$

where: Q_r - part of the contact load Q in the area of pure ball rolling, f - coefficients of rolling friction.
For the determination of contact loads Q_r we will use Figure 9. This part of the load Q_r which is responsible for the resistance due to rolling is obtained by integrating the (17) where a positive slip occurs:

$$Q_r = 4\frac{1.5Q}{\pi ab}\int_0^1\int_{\varphi_1}^{\pi/2} abr\sqrt{1-r^2}\,dr d\varphi = Q\left(1-\frac{2\varphi_1}{\pi}\right) \quad [N] \tag{33}$$

Whereas the reduction on the shaft $M_{(T)r}$ is:

$$\left(M_{(T)ri} + M_{(T)ro}\right)\omega_B = M_{(T)r}\omega \quad [mW] \tag{34}$$

Finally, the rolling resistance looks like follow:

$$M_{(T)r} = \frac{Q_i f_i\left(1-\frac{2\varphi_{1i}}{\pi}\right) + Q_o f_o\left(1-\frac{2\varphi_{1o}}{\pi}\right)}{M_B} \quad [Nmm] \tag{35}$$

To illustrate the share of individual components of resistance to motion due to sliding, spinning and rolling friction in the bearing, Figure 11 presents their comparison for the test bearing type FAG 7OB13-E, for the speed 12.000 rpm, preload 1000N.

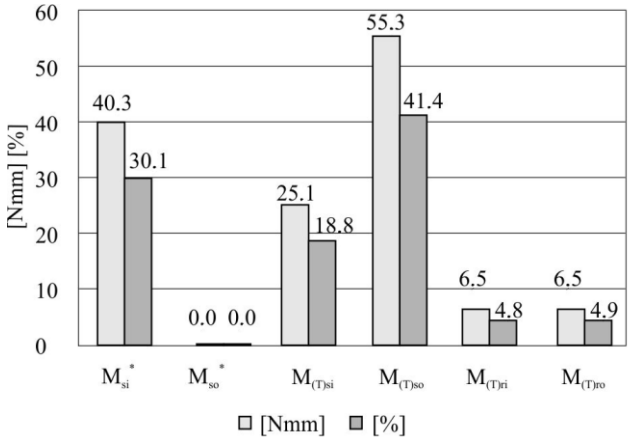

Fig. 11. Comparison of movement resistances in a bearing due to sliding, spinning and rolling friction

6. EXPERIMENTAL VERIFICATION OF COMPUTATIONAL MODELS

In our Department an experimental post was developed which allows for the measurement of torque on the ball bearing drive shaft (Muszynski and Kosmol, 2018). It is shown on Figure 12. Kistler torque sensor type 7292 is used for torque measurement and a Kistler sensor type 9102A for preload. The rotational speed was changed steplessly up to 10.000 rpm, and the preload up to 1000N.

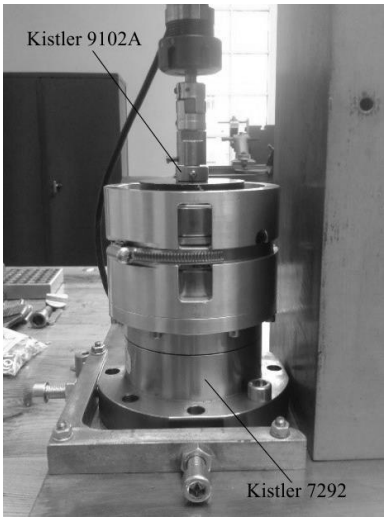

Fig. 12. View of the experimental post

Figure 13 shows an example of the study results as the influence of rotational speed on the total friction torque M_T of the angular-contact ball bearing.
By comparing the results of analytical and experimental studies an opinion on their qualitative compatibility can be formulated. However quantitative, the influence of rotational speed on the friction torque a little differs.

7. CONCLUSIONS

- Theoretical considerations concerning the motion in angular-contact ball bearing were presented in the article. It was assumed that analytical methods can be used to calculate the resistances as a function of the contact loads, bearing speed and preload only.

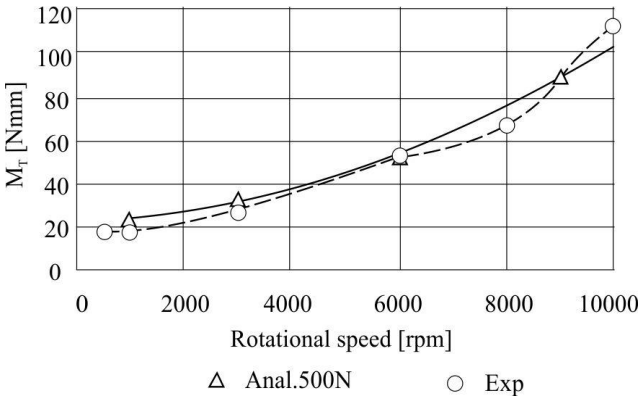

Fig. 13. Influence of rotational speed on the total friction torque of the angular ball bearing:
Anal.500N - analytical results for 500N preload,
Exp – experimental results

- As a result, a simple mathematical relationships were obtained, which combines friction torques due to spinning (31), sliding (29), (30) and rolling (35)

effects with normal contact loads Q_i and Q_o, rotational speed ω and preload F_a of bearing.
- The comparison of experimental and analytical results show that the developed models are sufficiently accurate for engineering needs.

8. REFERENCES

1. Harris Y., Kotzalas M., (2007). *Rolling Bearing Analysis 5th edn*: *Advanced Concepts of Bearing Technology*, London, TaylorandFrancis Group.
2. Houpert L., (1999). *Numerical and Analytical Calculations in Ball Bearings*, Timken Research Europe B.P. 89 680002 Colmar France.
3. Jones A.B., (1959). *Ball motion and sliding friction in ball bearings*, Journal of Basic Engineering Transactions of the ASME.
4. Kosmol J., (2019). *Extended contact model of angular bearing*, J. of Theoretical and Applied Mechanics, **57** (1), pp. 59-72.
5. Kosmol J., (2018). *Analytical determination of rolling friction coefficient of angular bearing*, J. of Manufacturing Science and Engineering, **140**, pp. 021002-1-021002-7.
6. Kosmol J., (2016). *Determination of Motion Resistances in High-Speed Spindle Angular Bearings*, Silesian University of Technology Publisher, Gliwice.
7. Muszyński M., Kosmol J., (2018). *Experimental studies on motion resistance in angular-contact ball bearings*, Inżynieria maszyn, **23**(1), pp. 36-44.
8. Noel D. at all, (2013). *Complete Analytical Expression of the Stiffness Matrix of Angular Contact Ball Bearing*, J. of Tribology, **135**(4).
9. Palmgren A., (1951). *Rolling bearing*, PWT, Warsaw.
10. Zama A., at all, (2019). *Advances in angular contact ball bearings testing machine design*, Int. J. of Modern Manufacturing Technologies, **XI**(3), pp. 137-142.

Received: February 09, 2021 / Accepted: June 15, 2021 / Paper available online: June 20, 2021